Radiol med (2017) 122:814–821
DOI 10.1007/s11547-017-0788-9

ABDOMINAL RADIOLOGY

Renal epithelioid angiomyolipoma: MRI findings

Yan Zhong[1] · Yanguang Shen[1] · Jingjing Pan[1] · Yingwei Wang[1] · Yunxia An[2] · Aitao Guo[2] · Lu Ma[1] · Huiyi Ye[1] · Haiyi Wang[1]

Received: 2 May 2017 / Accepted: 29 June 2017 / Published online: 10 July 2017

Abstract
Purpose To retrospectively analyze the MR imaging presentation of renal epithelioid angiomyolipoma (EAML).
Methods Retrospective analysis revealed 12 subjects with histologically proven renal EAML who underwent preoperative MRI at our institution between January 2009 and June 2016. Two radiologists reviewed the images in consensus, describing MR imaging features including size, location, growth pattern, signal intensity of tumor, and dynamic enhancement pattern.
Results Nine women and three men were included. The average maximum tumor diameter was 7.1 cm. Exophytic growth was present in 9/12 cases, mesophytic growth in 2/12, and endophytic growth in 1/12. On T1-weighted images, 2/12 displayed homogeneous isointensity, 1/12 homogeneous hyperintensity, 5/12 heterogeneous hypointensity, and 4/12 heterogeneous hyperintensity. Macroscopic fat was detected in 5/12 cases and microscopic fat in 6/12 cases. On T2-weighted images, 5/12 showed heterogeneous hypointensity, 4/12 heterogeneous hyperintensity, and 3/12 homogeneous hypointensity. On dynamic contrast-enhanced MR images, 7/12 showed a slow washout enhancement pattern, 2/12 a rapid washout pattern, 2/12 progressive enhancement, and 1/12 persistent enhancement. Imaging findings were suggestive of hemorrhage (50%), necrosis (25%), or cystic change (50%) within the tumors. Enlarged vessels were detected in 5/12 cases. One tumor extended into the renal sinus. No metastases were found on the preoperative MR imaging.
Conclusion Although MRI appearances of renal EAML were various, some MRI characteristics may contribute to suggest the possibility of renal EAML.

Keywords Angiomyolipoma · Renal epithelioid angiomyolipoma · Renal mass · Magnetic resonance imaging

Introduction

Renal angiomyolipoma (AML) is the most common benign solid renal tumor, accounting for 2.0–6.4% of all renal tumors [1–3]. On histology, AMLs are composed of varying amounts of mature adipose tissue, smooth muscle, and thick-walled blood vessels [4]. Renal AML is now considered to belong to the family of perivascular epithelioid cell tumors (PEComa) [5]. Renal epithelioid angiomyolipoma is a rare variant of AML that consists of variable portions of epithelioid cells [6]. Most cases of EAML follow a benign course, but about 1/3 of EAML cases display aggressive biological behavior or result in distant metastases to the lung, liver, and lymph nodes [4]. In 2004, the World Health Organization Classification of Renal Neoplasms considered EAML as a potentially malignant mesenchymal neoplasm [4].

Renal EAML can demonstrate different morphological patterns with carcinoma-like growth on histology, and can, therefore, be erroneously diagnosed as sarcoma or renal cell carcinoma (RCC) [7, 8]. Recently, Pan et al. found that EAML is activated through the mTOR pathway [9], and mTOR inhibitors such as sirolimus or temsirolimus have been considered as the best treatment option for patients

✉ Huiyi Ye
13701100368@163.com

✉ Haiyi Wang
wanghaiyi301@126.com

[1] Department of Radiology, Chinese PLA General Hospital, Fuxing Road 28, Box 100853, Beijing, China

[2] Department of Pathology, Chinese PLA General Hospital, Fuxing Road 28, Beijing, China

with EAML [10, 11]. To perform such optimal treatment, it is crucial that the preoperative imaging findings suggest the possibility of EAML. However, there have only been a few reports concerning the ultrasound, computed tomography (CT), or MRI features of renal EAML [12–14]. To the best of our knowledge, only two studies have reported on the conventional MR imaging features of EAML, and these included the low sample size of only 6 patients [12]. Correct preoperative diagnosis of renal EAML by imaging is difficult; this may be due to both a low incidence and a low level of awareness. Therefore, the objective of this study is to present the MR presentation of EAML to improve the understanding of this rare renal tumor.

Materials and methods

Patients

Our institutional review board approved this retrospective study and waived the requirement for informed consent. The pathology databases at our institution were searched to identify all cases of histologically proven renal EAML from March 2009 through June 2016. The search identified a total of 25 patients. Thirteen of these patients were excluded for the following reasons: only preoperative CT images were available ($n = 7$), and the absence of preoperative imaging at our institution ($n = 6$). Our final study included 12 patients who underwent preoperative MRI. One patient had another 3 conventional AMLs in the same kidney confirmed by surgery and pathology.

MR imaging sequences

MR imaging was performed on 1.5-T ($n = 10$, Signa HDXT, GE Healthcare, Milwaukee, WI) or 3.0-T systems ($n = 2$, Signa Excite, GE Healthcare) using a surface phased-array coil. The imaging sequence was: (a) axial T1-weighted dual echo out-of-phase and in phase sequences; (b) coronal and axial T2-weighted fast recovery fast spin echo fat saturation sequences; (c) a diffusion-weighted imaging (DWI) sequence using fat-suppressed single-shot echo-planar imaging with b values of 0 and 800 s/mm^2; (d) a transverse three-dimensional fat-suppressed T1-weighted gradient-echo sequence performed before and at three time points after contrast medium administration. Gadopentetate dimeglumine (Magnevist; Bayer, Leverkusen, Germany; 0.1 mmol/kg of body weight) was injected intravenously at a rate of 2 mL/s using a power injector (Medrad, Warrendale, PA, USA), and was followed by a 20 mL saline flush. The acquisition of the cortico-medullary phase was obtained 25–30 s after contrast material administration, the nephrographic phase at 60 s, and the excretory phase at 240 s.

Qualitative MR image analysis

All MR images were independently analyzed by two radiologists (with 5 and 10 years of experience in abdominal imaging), with the final decisions being reached by consensus. The following features of renal EAML were analyzed: (1) axial maximum diameter of the tumor; (2) location (upper pole, inter-polar, lower pole); (3) growth pattern (exophytic, mesophytic, endophytic); (4) signal intensity on in- and out-of-phase T1-weighted images; (5) signal intensity on T2-weighted images; (6) microscopic fat (signal drop areas on out-of-phase images corresponding to intermediate to hyperintensity on in phase T1-weighted images); (7) macroscopic fat (hyperintensity areas the same as the fat signal on in phase T1-weighted images, but signal suppressed on fat-suppressed T1-weighted images); (8) hemorrhage (hyperintense area of the tumor on fat-suppressed T1-weighted images); (9) necrosis (slight hyperintensity on T2-weighted images but lower than that of cerebrospinal fluid in the central part of the tumor; hypointense on T1-weighted images; no enhancement); (10) cystic change (signal intensity of the area the same as that of cerebrospinal fluid on both T1 and T2-weighted imaging; no enhancement on dynamic contrast imaging); (11) enhancement pattern; (12) predominant signal intensity on dynamic contrast images (on cortico-medullary, nephrographic, and excretory phases); (13) rupture; (14) enlarged vessels; (15) renal sinus invasion; (16) enlarged lymph nodes; and (17) metastasis.

Based on the ratio of solid and cystic components, the tumors were classified as solid type (including purely solid and solid with a minor cystic component), mixed solid and cystic-type (defined as approximately equal proportions of solid and cystic components), and multilocular cystic-type.

The signal intensity of the tumor was defined in comparison with the normal cortex and was described as hypo-, iso-, or hyperintensity for each MR imaging sequence. If the signal intensity of the tumor was heterogeneous, the predominant signal was used to represent the signal intensity of the tumor.

The enhancement pattern of the tumor on dynamic contrast-enhanced MR images from the cortico-medullary through nephrographic to excretory phases was defined as: I slow washout; II rapid washout; III progressive enhancement; IV persistent enhancement.

The reviewers also recorded the patients' age, sex, clinical symptoms, and nephrectomy method.

Pathological examination

Twelve surgical resection specimens were fixed in 10% formalin and stained with hematoxylin–eosin (HE). Immunohistochemical staining was performed with labeled antibodies for HBM-45, Melan-A, SMA, S-100, and Ki-67. Two pathologists reviewed all the samples in consensus.

Statistical analysis

All data were analyzed statistically using SPSS version 19.0 (IBM, Armonk, NY, USA). Quantitative data were expressed as the mean and range (minimum and maximum value). Spearman's correlation was performed between the size and hemorrhage status of the tumor.

Results

Clinical information

The clinical characteristics of the 12 patients are shown in Table 1. Nine patients were women, and three were men, with the mean age being 46 years (range 27–61 years). Patients presented as asymptomatic in seven cases, with symptoms including waist discomfort in 3 cases, and low back pain in 2 cases. No patients had tuberous sclerosis (TS). Three conventional AMLs were present in one patient. Four patients underwent radical nephrectomy, and 8 patients underwent partial nephrectomy. None of the patients had metastasis at the time of surgery. Eight patients were lost on follow-up, with the follow-up of the other 4 cases lasting 1–10 months.

Imaging findings

The imaging characteristics are summarized in Table 2. The mean maximal diameter was 7.1 cm (range 1.1–12.3 cm). Six lesions were in a left kidney and 6 in a right kidney. The lesions were located in the inter-polar region in eight cases and the lower pole in four cases. Nine out of twelve (75%) lesions displayed exophytic growth, 2/12 (17%) mesophytic growth, and 1/12 (8%) endophytic growth.

On T1-weighted images, 2/12 cases (17%) displayed homogeneous isointensity in comparison with the adjacent normal renal cortex, 5/12 (42%) heterogeneous hypointensity, 1/12 (8%) homogeneous hyperintensity, and 4/12 (33%) heterogeneous hyperintensity. Macroscopic fat on MR images was recognizable in 5/12 (42%) cases. Identifiable fat constituted more than 50% of the tumor volume in 1 case (Fig. 1), 90% in 1 case, 20–35% in 2 cases, and a small focus in 1 case. Microscopic fat was recognized as signal loss on opposed-phase MR images in 6/12 (50%) cases in comparison with the in phase T1-weighted images, while 5/12 (42%) cases contained macroscopic and microscopic fat. Hemorrhage was identified in 6/12 (50%) cases and constituted close to 50% of the tumor volume in 4 cases, but less than 25% of the tumor volume in the other 2 cases. In 1 tumor (maximum diameter of 8.7 cm), hemorrhage was secondary to rupture into the perirenal fat capsule and fascia planes. There was no correlation between size and hemorrhage of the tumor at diagnosis ($r = 0.197$, $P = 0.54$).

On T2-weighted images, 3/12 (25%) tumors displayed homogeneous hypointensity, 5/12 (42%) were heterogeneously hypointense, and 4/12 (33%) were heterogeneously hyperintense. A cystic change was identified in 6/12 (50%) tumors, which constituted less than 20% of the tumor volume in 2 cases, about 50% of the tumor volume in 3 cases, and more than 75% of the tumor volume in 1 case with a fluid–fluid level. Eight out of 12 (67%)

Table 1 Clinical features of renal epithelioid angiomyolipoma (EAML)

Patient	Age (years)	Gender	Symptom	Nephrectomy	Metastasis	Follow-up
1	48	M	Waist discomfort	Partial	Absent	Absent
2	43	F	Asymptomatic	Partial	Absent	Absent
3	39	F	Low back pain	Radical	Absent	Absent
4	51	F	Waist discomfort	Radical	Absent	Absent
5	48	F	Asymptomatic	Partial	Absent	Absent
6	55	F	Asymptomatic	Partial	Absent	5 months
7	33	F	Asymptomatic	Partial	Absent	10 months
8	50	F	Asymptomatic	Radical	Absent	1 month
9	45	F	Asymptomatic	Radical	Absent	1 month
10	27	M	Waist discomfort	Partial	Absent	Absent
11	61	F	Low back pain	Partial	Absent	Absent
12	49	F	Asymptomatic	Partial	Absent	Absent

Table 2 Imaging features of renal epithelioid angiomyolipoma (EAML)

Variable	Number of patients ($n = 12$)	%
Location		
Upper pole	0	0
Inter-polar	8	67
Lower pole	4	33
Growth pattern		
Exophytic	9	75
Mesophytic	2	17
Endophytic	1	8
Lesion classification		
Solid type	8	67
Mixed solid and cystic-type	3	25
Multilocular cystic-type	1	8
Macroscopic fat	5	42
Microscopic fat	6	50
Cystic degeneration	6	50
Necrosis	3	25
Hemorrhage	6	50
T1-weighted image		
Homogeneous isointensity	2	17
Heterogeneous hypointensity	5	42
Homogeneous hyperintensity	1	8
Heterogeneous hyperintensity	4	33
T2-weighted image		
Homogeneous hypointensity	3	25
Heterogeneous hypointensity	5	42
Heterogeneous hyperintensity	4	33
DWI		
Heterogeneous hyperintensity	11	92
Hypointensity	1	8
Enhancement pattern		
Rapid washout	2	17
Slow washout	7	58
Progressive enhancement	2	17
Persistent enhancement	1	8
Enlarged lymph node	0	0
Enlarged vessels	5	42
Rupture	1	8
Renal sinus invasion	1	8

cases were of a solid type (Fig. 2), 3/12 (25%) cases a mixed solid and cystic-type (Fig. 3), and 1 (8%) case was of a multilocular cystic-type. The solid component and septa showed hypointensity. The central part of 3/12 (25%) cases presented necrosis.

On DWI, 11 tumors demonstrated heterogeneous hyperintensity, while 1 predominantly fat tumor demonstrated hypointensity.

On dynamic contrast-enhanced MR images, the enhancement degree varied from mild through moderate to obvious. One (8%) tumor showed a mild homogeneous enhancement with persistent enhancement, 2/12 (17%) an obvious homogenous pattern with rapid washout, 7/12 (58%) a moderate heterogeneous enhancement with a slow washout pattern, and 2/12 (17%) a moderate heterogeneous enhancement with progressive enhancement. Enlarged vessels were seen in 5/12 (42%) cases.

One tumor extended into the renal sinus. Renal pelvises were compressed and dilated in 2 cases. None of the cases had enlarged lymph nodes or renal venous thrombosis. No metastases were found on the preoperative MR imaging.

Pathologic findings

The epithelioid cells were seen in all cases. In the immunohistochemical analysis, HMB-45 and smooth-muscle actin (SMA) were positive, while epithelial markers were negative in all cases. Melan-A was positive in all cases except one. Invasion of the renal capsule was present in 1 case (8%) and invasion of the perirenal fat capsule was present in another case. No cases had distant metastasis or vascular invasion. Four out of 12 cases showed more than 10% positivity for Ki-67.

Discussion

Renal EAML is a rare mesenchymal tumor occurring mainly in adults. Even though EAML affects both men and women [4], it predominantly occurs in women [12–14]. In our study, there were 9 female patients and 3 male patients, which present a ratio consistent with a previous study. The tumor size is typically large [12, 15, 16], which is in accordance with our results. Exophytic growth is one of the characteristics of EAML; the pathological basis for this may be that the infiltrating ability of the benign tumor is lower in the parenchyma, but that it can easily grow in the relatively low resistance of the renal interlobular tissue. In the present study, 9/12 cases displayed exophytic growth, which is consistent with the study of Froemming et al. (8/9 lesions showed complete exophytic growth) [12].

Aydin et al. [17] reported that multiple AML and cysts are the most common manifestation in TS. Lane et al. [18] reported that 12 of 85 patients with multiple AML had a definite diagnosis of TS. Although 1 case in the present study had 3 additional AMLs, no other manifestations confirmed

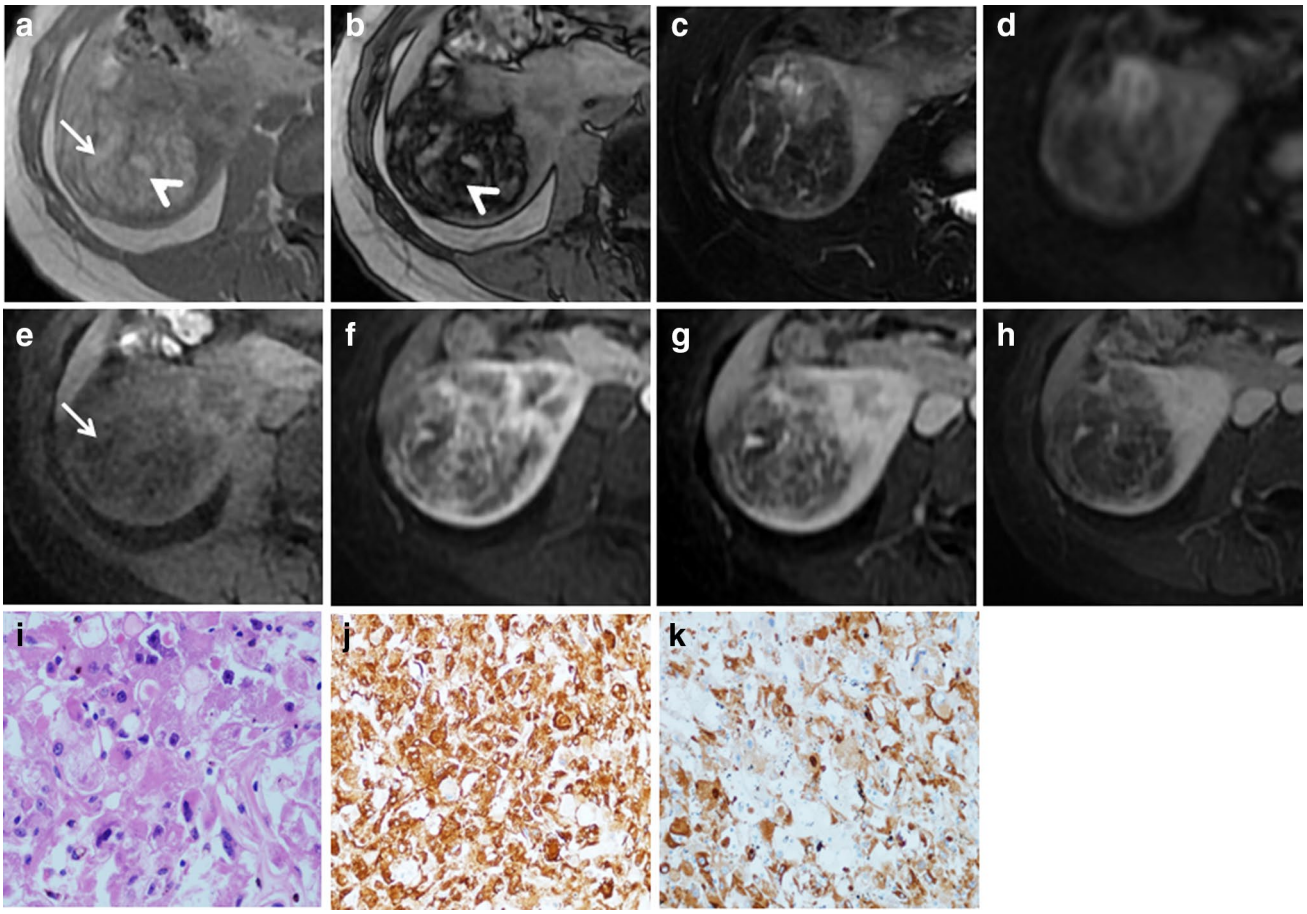

Fig. 1 A 33-year-old asymptomatic woman with right renal EAML. **a** On the in phase image the lesion shows heterogeneous hyperintensity. **b** On the out-of-phase image the signal intensity of the lesion is markedly decreased, indicating microscopic fat (*arrowhead*). **c** On the T2-weighted image the lesion shows heterogeneous hypointensity. **d** On the DWI the lesion shows heterogeneous hyperintensity. **e** On the fat-suppressed T1-weighted image the hyperintense area of the lesion on the in phase image shows as a hypointensity, indicating macroscopic fat (*arrow*). **f** On the cortico-medullary phase image the lesion shows heterogeneous moderate enhancement. **g–h** From the nephrographic to excretory phase the lesion shows a slow washout pattern. **i** Photomicrographs (HE staining, ×400) show multiple epithelioid cells. **j–k** Immunohistochemical stainings (×200) for HMB-45 and Melan-A are positive

the patient as having TS. Patients with a small EAML tumor commonly have no specific clinical symptoms; the tumors are incidentally detected by imaging examinations performed as a part of routine health checks or unrelated examinations. Patients suffer from abdominal discomfort or pain when the tumor is large or presents with rupture. In our study, 7 patients were asymptomatic, 3 patients presented with waist discomfort, and 2 patients with waist pain.

Unlike classic AML, most EAML tumors contain few or no fat cells [19–22].Tsukada et al. reported that intratumoral fat was not detected in any of their cases on MR imaging [22], while Froemming et al. reported that fat was detected in 5 cases on CT or MR imaging, and that microscopic fat was detected in one additional case [16]. In the present study, macroscopic fat was detected in 5/12 cases and microscopic fat in 6/12 cases. We, therefore, found that the presence of macroscopic fat was not specific to the diagnosis of classic AML, with the presence of macroscopic fat being similar in hepatic EAML [23].

In previous studies, the signal intensity or density of the majority of EAMLs was described as heterogeneous on MR or CT imaging [12, 13, 16, 22], with the causes for this being given as hemorrhage, necrosis, or cystic change. In our study, hemorrhage was identified in 6/12 cases, necrosis in 3 cases, and cystic change in 6 cases, which are rates consistent with previous studies. Meanwhile, EAML tends to be hemorrhage and secondary to rupture and presents with a peripheral hematoma. In the study by Froemming et al. 3 of the 4 hemorrhaging EAML tumors ruptured with a perinephric hematoma [12], while Tsukada et al. found that 1 of their 8 tumors showed a spontaneous perirenal hematoma [22]. In our study, 1 of the 5 hemorrhaging EAML tumors ruptured, and this was accompanied by a perinephric hematoma. AML is one of the most common renal tumors with

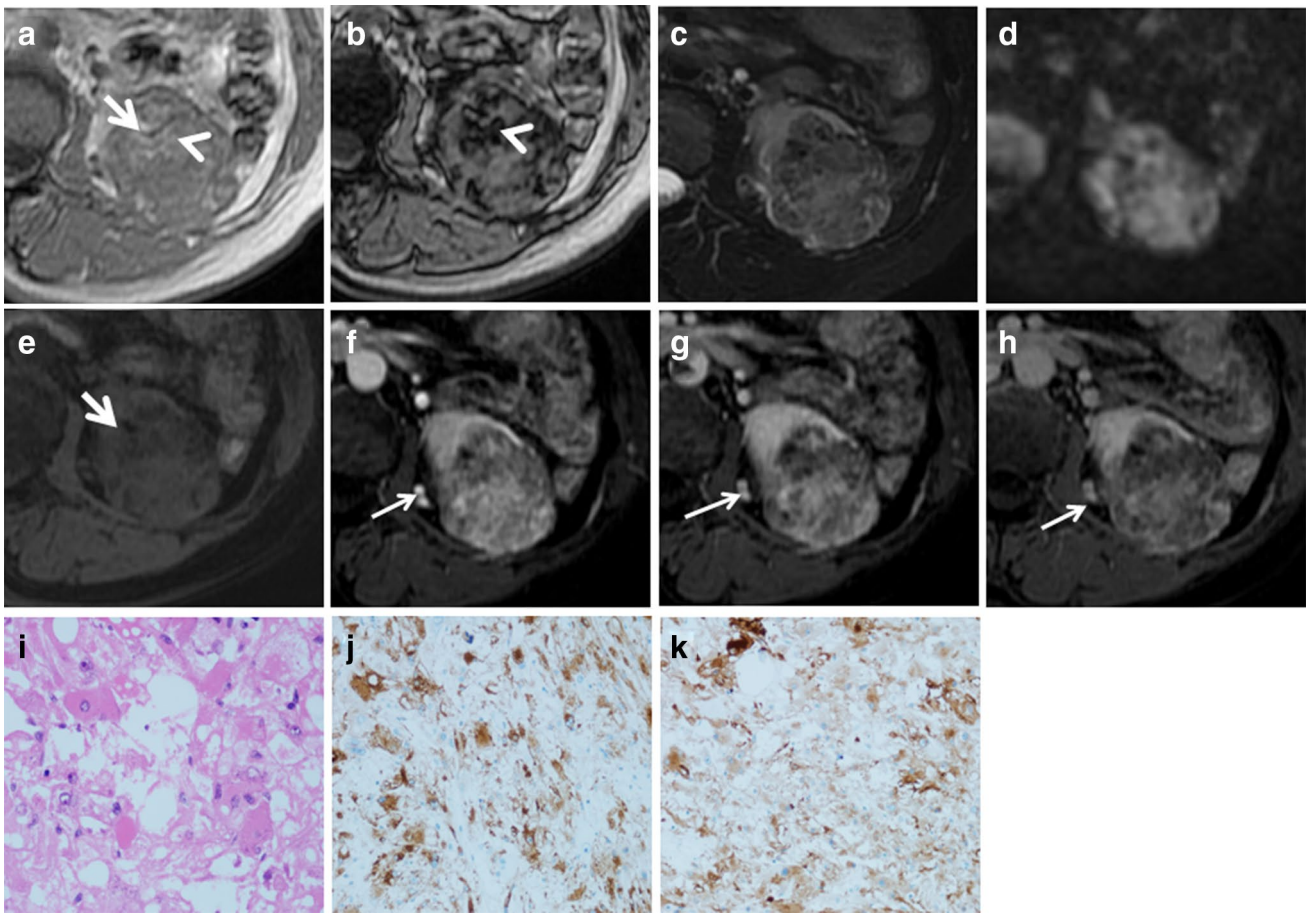

Fig. 2 A 43-year-old asymptomatic woman with left lower pole renal EAML. **a** On the in phase image the lesion shows heterogeneous hyperintensity. **b** On the out-of-phase image the signal intensity of the lesion is markedly decreased, indicating microscopic fat (*arrowhead*). **c** On the T2-weighted image the lesion shows heterogeneous hypointensity. **d** On DWI the lesion shows heterogeneous hyperintensity. **e** On the fat-suppressed T1-weighted image the focal hyperintense area of the lesion on the in phase image shows as a hypointensity, indicating macroscopic fat (*short arrow*). **f** On the cortico-medullary phase image the lesion shows heterogeneous moderate enhancement with enlarged vessels (*long arrow*). **g–h** From the nephrographic phase to excretory phase the lesion shows a slow washout pattern. **i** Photomicrographs (HE staining, ×400) show multiple epithelioid cells. **j-k** Immunohistochemical stainings (×200) for HMB-45 and Melan-A are positive

the ability to cause spontaneous perirenal hematoma [24], with a second being RCC. Other renal tumors including metastatic tumors of malignant melanoma, renal abscesses, ruptured renal cysts, and pheochromocytomas, also cause spontaneous perirenal hematoma [24]. Therefore, EAML should be listed in the differential diagnosis of spontaneous perirenal hematoma of renal tumors. AML ≥4 cm has a 50% risk of hemorrhage [25, 26], but although EAML tumors tend to be relatively large at diagnosis, we found no significant correlation between the size of the tumor and hemorrhage of the tumor at diagnosis (P >0.05).

The solid component of EAML commonly displays hypointensity on T2-weighted images. The possible pathological basis for this is the evident number with a (in this case epithelioid) muscle component [22]. A previous study found that 3/4 cases displayed hypointensity on T2-weighted MR images [22], and in our study, 8/12 cases displayed hypointensity. EAML can present with either predominantly solid type lesions or predominantly cystic-type lesions [22]. Our data showed that 3/12 cases had a mixed solid and cystic-type, 1 case had a multilocular cystic-type, and 8 cases a solid type. The cystic-type mimicked multilocular cystic renal neoplasm of low malignant potential. No previous study has described the DWI findings. Although most of the lesions in our data displayed obvious diffusivity, the DWI findings were non-specific. The degree of diffusivity is determined by the components of the tumor and is reflected by the apparent diffusion coefficient (ADC) value.

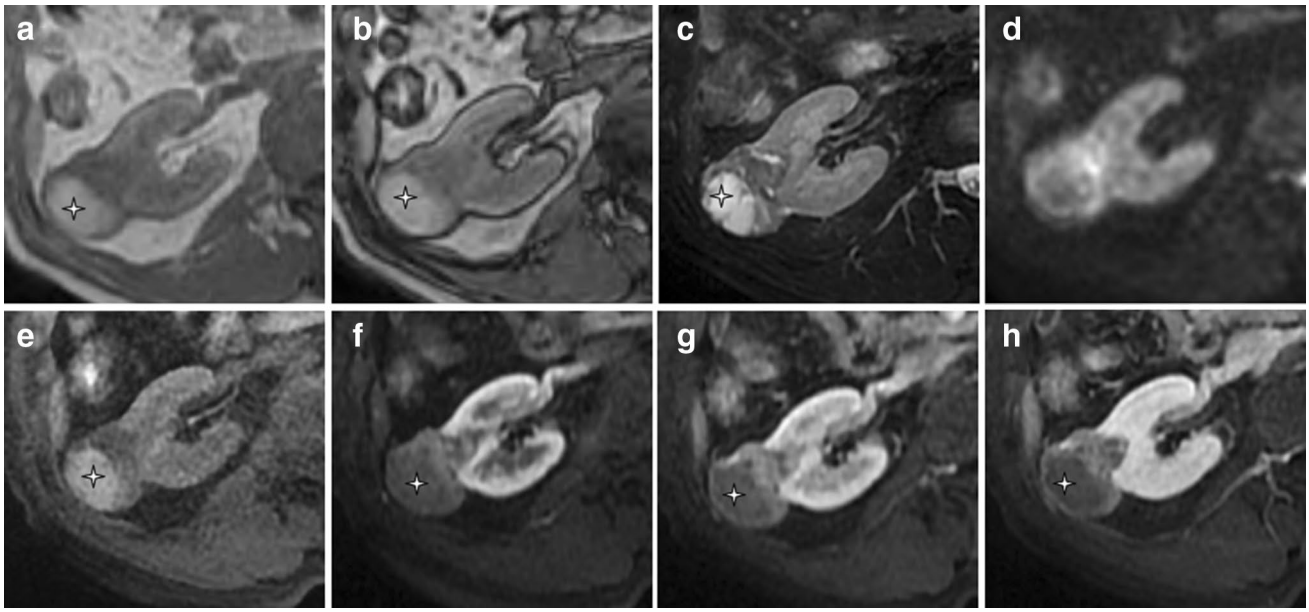

Fig. 3 A 45-year-old asymptomatic man with right renal EAML. **a** On the in phase image the lesion shows heterogeneous hyperintensity with exophytic growth. **b** On the out-of-phase image the signal intensity of the lesion does not change in comparison with the in phase image. **c** On the T2-weighted image the lesion shows heterogeneous hypointensity and hyperintensity. **d** On DWI the lesion shows heterogeneous hyperintensity. **e** On the fat-suppressed T1-weighted image the lesion shows heterogeneous hyperintensity and hypointensity, with the hyperintense area indicating a hemorrhage (*star*). **f** On the cortico-medullary phase image the solid part of the lesion shows heterogeneous moderate enhancement. **g–h** From the nephrographic phase to excretory phase the lesion shows a slow washout pattern

On the dynamic contrast-enhanced images, the enhancement patterns were non-specific, with the degree of enhancement also varying [12, 22]. In the study by Froemming et al. 3 of the 5 cases showed mild enhancement, and 2 showed moderate to marked enhancement. In the present study, 7/12 cases showed a slow washout and 2/12 a rapid washout pattern; these enhancement patterns are similar to those of AML [27]. Two other cases displayed a progressive enhancement pattern, and 1 displayed a persistent enhancement pattern. This variety of enhancement patterns in EAML is also similar to that for AML with no visible fat. The enhancement pattern and degree may depend on the components of the tumor [28].

An enlarged vessel is also characteristic of EAML. Six of the 9 lesions in the study by Froemming et al. presented with enlarged vessels [12] and 5/12 cases displayed enlarged vessels in our study. However, not all imaging studies have reported this sign [14, 16, 22].

Approximately a third of EAML cases have been found to present with malignant biological behaviors [4]. In one study, 2 tumors were locally invasive, and 1 patient had metastatic disease at presentation [12], while in another study, 1 of the 10 tumors demonstrated retroperitoneal lymphadenopathy [16], and in a third study a thrombus was present in the right renal vein, but none of the cases displayed metastases [22]. In our study, although 1 case showed renal sinus invasion on MR imaging; 1 case an invaded renal capsule, and 1 case perirenal fat on pathology, other aggressive signs, such as metastases, enlarged lymph nodes, or thrombus, were not found on the preoperative MR imaging. The follow-up on 4 patients also showed no recurrences or metastases.

On histology, EAML consists of predominantly epithelioid cells and abundant multi-nucleated giant cells, with minimal or no adipose tissue, while the diagnosis of EAML depends on the detection of epithelioid cells. On immunohistochemical analysis, EAML shows similarities with classic AML; the melanocytic markers (e.g., HMB-45, melan-A) and smooth muscle markers (e.g., smooth-muscle actin) are positive, while the epithelial markers are negative [6]. In contrast, RCCs are positive for epithelial markers and negative for melanocytic markers [17]. The clinical significance of Ki-67 as a proliferative cell and prognostic marker has also been investigated in human tumors [29]. In EAML with metastasis there is a strong positive expression of Ki-67 [30]. In our study, 4 out of 12 cases of EMAL showed more than 10% positivity for Ki-67 index, with 2 cases showing local invasion on pathology.

Our study had some limitations; first, the study is retrospective in nature. Second, the sample size is relatively small because of the rarity of the tumor. Third, 8 of the 12 patients did not receive follow-up.

In summary, renal EAML is a potentially malignant mesenchymal tumor. Renal EAMLs demonstrate a range

of MR appearances, and sometimes, it is difficult to distinguish renal EAML from classic AML or renal cell tumor by MRI features. However, according to the present study, these features include a large size, exophytic growth, minimal macroscopic fat, microscopic fat, massive hemorrhage, enlarged vessels, and hypointensity on T2-weighted images, may help to identify renal EAML. The definitive diagnosis of renal EAML still currently depends on pathology.

Compliance with ethical standards

Conflict of interest The authors declare that they have no conflict of interest.

Ethical standards This article does not contain any studies with human participants performed by any of the authors. Each author has participated sufficiently in any submission to take public responsibility for its content. Institutional Review Board approval was obtained and written informed consent was waived by the Institutional Review Board.

References

1. Game X, Soulie M, Moussouni Roux D, Escourrou G, Chevreau C et al (2003) Renal angiomyolipoma associated with rapid enlargement [correction of enlargement] and inferior vena caval tumor thrombus. J Urol 170:918–919
2. L'Hostis H, Deminiere C, Ferriere JM, Coindre JM (1999) Renal angiomyolipoma. a clinicopathologic, immunohistochemical, and follow-up study of 46 cases. Am J Surg Pathol 23:1011–1120
3. Tallarigo C, Baldassarre R, Bianchi G, Comunale L, Olivo G, Pea M et al (1992) Diagnostic and therapeutic problems in multicentric renal angiomyolipoma. J Urol 148:1880–1884
4. Eble JN, Sauter G, Epstein JI, Sesterhenn IA (2004) World Health Organization classification of tumours: pathology and genetics of tumours of the urinary system and male genital organs. IARC, Lyon
5. Folpe AL, Kwiatkowski DJ (2010) Perivacular epithelioid cell neoplasia: pathology and pathogenesis. Hum Pathol 41:1–15
6. Katabathina VS, Vikram R, Nagar AM, Tamboli P, Menias CO, Prasad SR (2010) Mesenchymal neoplasms of the kidney in adults: imaging spectrum with radiologic-pathologic correlation. Radiographics 30(6):1525–1540
7. Belanger EC, Dhamanaskar PK, Mai KT (2005) Epithelioid angiomyolipoma of the kidney mimicking renal sarcoma. Histopathology 47:433–435
8. Svec A, Velenska Z (2005) Renal epithelioid angiomyolipoma-a close mimic of renal cell carcinoma. Report of a case and review of the literature. Pathol Res Pract 200:851–856
9. Pan CC, Chung MY, Ng KF, Liu CY, Wang JS, Chai CY et al (2008) Constant allelic alteration on chromosome 16p (TSC2 gene) in perivascular epithelioid cell tumour (PEComa): genetic evidence for the relationship of PEComa with angiomyolipoma. J Pathol 214:387–393
10. Wolff N, Kabbani W, Bradley T, Raj G, Watumull L, Brugarolas J (2010) Sirolimus and temsirolimus for epithelioid angiomyolipoma. J Clin Oncol 28:e65–e68
11. Shitara K, Yatabe Y, Mizota A, Sano T, Nimura Y, Muro K (2011) Dramatic tumor response to everolimus for malignant epithelioid angiomyolipoma. Jpn J Clin Oncol 41:814–816
12. Froemming AT, Boland J, Cheville J, Takahashi N, Kawashima A (2013) Renal epithelioid angiomyolipoma: imaging characteristics in nine cases with radiologic-pathologic correlation and review of the literature. AJR Am J Roentgenol 200:W178–W186
13. Ryan MJ, Francis IR, Cohan RH, Davenport MS, Weizer A, Hafez K (2013) Imaging appearance of renal epithelioid angiomyolipomas. J Comput Assist Tomogr 37:957–961
14. Liu Y, Qu F, Cheng R, Ye Z (2015) CT-imaging features of renal epithelioid angiomyolipoma. World J Surg Oncol 13:280
15. Bharwani N, Christmas TJ, Jameson C, Jameson C, Moat N, Sohaib SA (2009) Epithelioid angiomyolipoma: imaging appearances. Br J Radiol 82:e249–e252
16. Cui L, Zhang JG, Hu XY, Fang XM, Lerner A, Yao XJ et al (2012) CT imaging and histopathological features of renal epithelioid angiomyolipomas. Clin Radiol 67:e77–e82
17. Aydin H, Magi-Galluzzi C, Lane BR, Sercia L, Lopez JI, Rini BI et al (2009) Renal angiomyolipoma: clinicopathologic study of 194 cases with emphasis on the epithelioid histology and tuberous sclerosis association. Am J Surg Pathol 33:289–297
18. Lane BR, Aydin H, Danforth TL, Zhou M, Remer EM, Novick AC et al (2008) Clinical correlates of renal angiomyolipoma subtypes in 209 patients: classic, fat poor, tuberous sclerosis associated and epithelioid. J Urol 180:836–843
19. Eble JN, Amin MB, Young RH (1997) Epithelioid angiomyolipoma of the kidney: a report of five cases with a prominent and diagnostically confusing epithelioid smooth muscle component. Am J Surg Pathol 21:1123–1130
20. Park HK, Zhang S, Wong MK, Kim HL (2007) Clinical presentation of epithelioid angiomyolipoma. Int J Urol 14:21–25
21. Warakaulle DR, Phillips RR, Turner GD, Davies D, Protheroe AS (2004) Malignant monotypic epithelioid angiomyolipoma of the kidney. Clin Radiol 59:849–852
22. Tsukada J, Jinzaki M, Yao M, Nagashima Y, Mikami S, Yashiro H et al (2013) Epithelioid angiomyolipoma of the kidney: radiological imaging. Int J Urol 20:1105–1111
23. O'Malley ME, Chawla TP, Lavelle LP, Cleary S, Fischer S (2017) Primary perivascular epithelioid cell tumors of the liver: CT/MRI findings and clinical outcomes. Abdom Radiol (NY). doi:10.1007/s00261-017-1074-y
24. Zhang JQ, Fielding JR, Zou KH (2002) Etiology of spontaneous perirenal hemorrhage: a meta-analysis. J Urol 167:1593–1596
25. Kim JK, Kim SH, Jang YJ, Ahn H, Kim CS, Park H et al (2006) Renal angiomyolipoma with minimal fat: differentiation from other neoplasms at double echo chemical shift FLASH MR imaging. Radiology 239:174–180
26. Halpenny D, Snow A, McNeill G, Torreggiani WC (2010) The radiological diagnosis and treatment of renal angiomyolipomas—current status. Clin Radiol 65:99–108
27. Vargas HA, Chaim J, Lefkowitz RA, Lakhman Y, Zheng J, Moskowitz CS et al (2012) Renal cortical tumors: use of multiphasic contrast-enhanced MR imaging to differentiate benign and malignant histologic subtypes. Radiology 264:779–788
28. Pedrosa I, Sun MR, Spencer M, Genega EM, Olumi AF, Dewolf WC et al (2008) MR imaging of renal masses: correlation with findings at surgery and pathologic analysis. Radiographics 28:985–1003
29. Gerdes J, Schwab U, Lemke H, Stein H (1983) Production of a mouse monoclonal antibody reactive with a human nuclear antigen associated with cell proliferation. Int J Cancer 31:13–20
30. Ooi SM, Vivian JB, Cohen RJ (2009) The use of the Ki-67 marker in the pathological diagnosis of the epithelioid variant of renal angiomyolipoma. Int Urol Nephrol 41(3):559–565